Available online at www.sciencedirect.com

SciVerse ScienceDirect

journal homepage: www.elsevier.com/locate/he

A more efficient anode microstructure for SOFCs based on proton conductors

Ben H. Rainwater [1], *Mingfei Liu* [1], *Meilin Liu**

Center for Innovative Fuel Cell and Battery Technologies, School of Materials Science and Engineering, Georgia Institute of Technology, 771 Ferst Drive, N.W., Atlanta, GA 30332, USA

ARTICLE INFO

Article history:
Received 28 June 2012
Received in revised form
1 September 2012
Accepted 4 September 2012
Available online 9 October 2012

Keywords:
SOFC
Anode
Microstructure
Proton conductor
Porosity
Fuel cell

ABSTRACT

While the desired microstructure of the state-of-the-art Ni-YSZ anode for a solid oxide fuel cell (SOFC) based on YSZ is well known, the anode microstructure for a SOFC based on a proton conductor is yet to be optimized. In this study, we examined the effect of anode porosity on the performance of a SOFC based on $BaZr_{0.1}Ce_{0.7}Y_{0.1}Yb_{0.1}O_{3-\delta}$ (BZCYYb), a mixed ion (proton and oxygen anion) conductor with high ionic conductivity at intermediate temperatures. Three cells with Ni-BZCYYb cermet anodes of different porosities (37%, 42%, and 50%) and identical electrolytes and cathode components were fabricated and tested. Under typical fuel cell operating conditions, the cell with anode of the lowest porosity (37%), prepared without pore former, achieved the highest performance, demonstrating a peak power density of 1.2 W/cm^2 at 750 °C. This is radically different from the results of Ni-YSZ anodes for YSZ based cells, where high anode porosity (~55%) is necessary to achieve high performance. The observed increase in performance (or electrocatalytic activity for anode reactions) is attributed primarily to the unique microstructure of the anode fabricated without the use of pore forming precursors.

1. Introduction

Fuel cells are devices that convert chemical energy to electrical energy and heat directly, and reduce greenhouse gas emissions when compared to conventional technologies [1]. Among all types of fuel cells, solid oxide fuel cells (SOFCs) have the potential to offer the highest chemical to electrical energy conversion efficiency, and have the flexibility to use a wide range of fuels, including hydrocarbons, coal gas, biomass, and other renewable fuels [2–6]. In state-of-the-art SOFCs, yttria-stabilized zirconia (YSZ) is used for the electrolyte due to its high ionic conductivity in the temperature range 800 °C-1000 °C, excellent chemical stability, good mechanical strength, and ease of fabrication. However, the conductivity of YSZ decreases rapidly as the temperature is reduced, making it unsuitable for intermediate temperature SOFCs (IT-SOFCs). New electrolyte materials based on doped barium cerate and zirconate, such as BZCY [7] and BZCYYb [8], have attracted wide attention due to high ionic conductivity at intermediate temperatures (450 °C–750 °C). These materials are mixed ion conductors, allowing transport of both proton and oxygen anion. Their transference numbers depend on composition and testing conditions. Under typical fuel cell operating conditions the $BaCeO_3$-based SOFCs have significant proton conduction. The high ionic conductivity at intermediate temperatures originates from the low activation energy for

* *Corresponding author*. Tel.: +1 404 894 6114; fax: +1 404 894 9140.
E-mail address: meilin.liu@mse.gatech.edu (M. Liu).
[1] The authors contributed equally to this work.
0360-3199/$ – see front matter
http://dx.doi.org/10.1016/j.ijhydene.2012.09.027

protonic defect transport (approximately 0.4–0.6 eV [9]) when compared to that for oxygen vacancy transport (approximately 1.1 eV [10]) [7,11]. $BaCeO_3$-based proton conducting electrolytes, particularly, have been studied extensively for use in IT-SOFCs [7,12–15].

SOFC anodes are commonly composed of nickel, which is inexpensive but electrocatalytically active for hydrogen oxidation at SOFC operating temperatures [16]. Cermet anodes are fabricated by mixing NiO and an ionically conducting oxide (e.g., an electrolyte) followed by reduction of NiO to Ni(metal) upon exposure to a fuel during the first hours of SOFC operation. Reduction of NiO creates porosity in the anode which is needed for gas-phase diffusion. The contiguous nickel metal creates electronic conduction pathways throughout the anode. Both porosity and electronic conduction are critical for the functions of a SOFC anode. The ion-conducting phase of the cermet anode, often identical to the electrolyte material of the cell to match TECs, forms a framework primarily responsible for structural support of the cell, maintenance of anode microstructure throughout the lifetime of cell operations, intimate contact with the dense electrolyte, and extension of the triple phase boundaries (gas, electronic conductor, ionic conductor) into the porous anode to increase the number of active sites for fuel oxidation [17,18]. In the literature $BaZr_{0.1}Ce_{0.7}Y_{0.1}Yb_{0.1}O_{3-\delta}$ (BZCYYb) [8] has been used successfully as the ceramic component of the cermet anode for SOFCs. The Ni-BZCYYb cermet anode also demonstrated resistance to coking and sulfur poisoning under hydrocarbon and H_2S contaminated fuels [8].

The state-of-the-art YSZ based oxygen anion conducting SOFC has been widely studied. The effect of anode microstructure (such as porosity, pore size, anode support thickness, and Ni to YSZ ratio) of a Ni-YSZ cermet anode on fuel cell performance has been systematically investigated [19–21]. For example, the optimal porosity in the Ni-YSZ cermet anode is higher than the porosity that is formed simply from the reduction of NiO. Higher porosity is achieved by adding pore formers, such as graphite, carbon black, or corn starch, in the early fabrication steps which burn out from the substrate during sintering in air, leaving pores for gas diffusion. In a thorough parameter investigation [20] of a YSZ-based cell, the Ni-YSZ cermet anode porosity was varied between 32% and 76%, in four test cells, by controlling the amount of pore former added to the precursor powders. With other parameters held constant, the peak power density varied from ~0.72 W/cm^2 for a cell with anode porosity of 32% to ~1.55 W/cm^2 for a cell with anode porosity of 57%; the increase in porosity significantly enhanced the performance [20]. This study, as well as others [19], require that pore formers be added in oxygen anion conducting SOFC anodes to create adequate porosity (~55%) to achieve high cell performance.

Proton conducting SOFCs differ from oxygen anion conducting SOFCs by where the products of the overall fuel cell reaction are formed. In oxygen anion conducting SOFCs, water is formed at the anode, diluting the fuel and thus reducing the Nernst potential. In contrast, water develops at the cathode in proton conducting SOFCs and the fuel remains pure. During routine operation, excess air is present at the cathode, therefore water formation at the cathode in proton conducting SOFCs has a minimal effect on cell voltage [22,23]. Because cell reaction water is formed at the cathode in proton conducting SOFCs, less porosity is needed for water diffusion when compared to oxygen anion conducting SOFCs. Although $BaZr_{0.1}Ce_{0.7}Y_{0.1}Yb_{0.1}O_{3-\delta}$ (BZCYYb) has partial oxygen anion conduction when used as the electrolyte in IT-SOFCs, much less water will be formed at the anode due to significant proton conduction.

Due to the difference of water formation location in proton conducting and oxygen anion conducting SOFCs, anodes with different porosities must be used in each type of SOFC to optimize performance. However, in the work of proton conductor based anode supported cells, 20 wt%-25 wt% pore former has been used in the anode support, in keeping with the conventional SOFC anode porosity used in YSZ-based cells [24,25], and the reported performance is not high. Even though some optimization of the anode microstructure has been done, such as adding an anode functional layer between the anode and electrolyte to improve the interface, the performance remains low (~300 mW/cm^2 at 700 °C) [24].

A recent study [17] revealed the unique microstructure that is formed when no pore formers are used in the nickel-cermet anode fabrication process using the commonly studied mixed conductor, $BaZr_{0.6}Ce_{0.2}Y_{0.2}O_{3-\delta}$. However, the material was not tested in an electrochemical device and the electrochemical properties of the microstructure were not studied. A study of correlation between microstructure and electrochemical performance in proton conducting anode supported SOFCs is lacking in the literature.

In this work, we investigated the effect of anode porosity on the performance of proton conducting SOFCs based on BZCYYb. Cells with Ni-BZCYYb cermet anodes of varying porosity are fabricated and tested. A sample with 50% anode porosity was fabricated for comparison to the optimized YSZ cell in the literature. However, high performance is observed in the SOFCs with anodes of low porosity (37%). This is in stark contrast to the conventional anode porosity (~55%) optimization trend for YSZ-based, oxygen anion conducting SOFCs. This work provides a new understanding for the rational development of high performance, intermediate temperature SOFCs based on proton conducting electrolytes.

2. Experimental

2.1. Sample preparation

$BaZr_{0.1}Ce_{0.7}Y_{0.1}Yb_{0.1}O_{3-\delta}$ (BZCYYb) was prepared by the solid–state reaction method from barium carbonate (Sigma Aldrich, ≥99%, $BaCO_3$), zirconium oxide (Alfa Aesar, 99%, ZrO_2), cerium(IV) oxide (Aldrich, 99.9%, CeO_2), yttrium(III) oxide (Alfa Aesar, 99.99%, Y_2O_3), and ytterbium(III) oxide (Alfa Aesar, 99.9%, Yb_2O_3) precursor powders in stoichiometric ratio. Powders were ball-milled for 24 h in ethanol, dried for 24 h, crushed, and calcined at 1100 °C for 10 h. The process was repeated to achieve the pure perovskite phase. The cermet anode was prepared by mixing nickel oxide (Alfa Aesar, NiO) and BZCYYb powders. The NiO and BZCYYb powders were ball milled in ethanol for 24h to achieve a homogeneous mixture, then dried. The nickel oxide to BZCYYb ratio was adjusted so that the Ni (metal) to BZCYYb volume ratio was 1:1 in all

samples after reduction. Three separate samples, containing 0 wt%, 10 wt% and 20 wt% corn starch pore former, were prepared from the NiO–$BaZr_{0.1}Ce_{0.7}Y_{0.1}Yb_{0.1}O_{3-\delta}$ mixture. These samples are labeled Ni-BZCYYb-0, Ni-BZCYYb-10, Ni-BZCYYb-20.

Button cells were fabricated by unixaial pressing (124 MPa) anode supports (d = 13 mm) with thickness of ~1 mm. The anode supports were fired at 800 °C for 2h to remove pore formers. The sample containing no pore former (Ni-BZCYYb-0) was also fired at 800 °C for consistency, although it was not necessary to remove pore former. The $BaZr_{0.1}Ce_{0.7}Y_{0.1}Yb_{0.1}O_{3-\delta}$ electrolyte membrane was prepared by a particle suspension coating process [26] on the anode supports followed by co-firing at 1400 °C for 5h to achieve a high density electrolyte. The final electrolyte thickness was ~15 μm. For the anode microstructure specific tests, the anodes were fired under the same conditions but without electrolyte. For full cell preparation, $La_{0.6}Sr_{0.4}Co_{0.2}Fe_{0.8}O_{3-\delta}$ (LSCF, Fuel Cell Materials)-BZCYYb (7:3 weight ratio) powders were mixed with V-006 and acetone to form a cathode slurry, which was brush-painted on the BZCYYb electrolyte, followed by firing at 1000 °C for 2h to form a porous LSCF-BZCYYb cathode on the BZCYYb electrolyte supported cell with an effective cathode area of 0.3 cm^2. The same cathode was used in each cell to compare the change in performance based on changes in anode microstructure alone. Silver wire and silver paste (Heareus) was used for current collection.

Bar samples (16 mm × 3.3 mm × 2.15 mm) were prepared by uniaxial pressing of the NiO-BZCYYb-0, NiO-BZCYYb-10, and NiO-BZCYYb-20 anode powders for electrical conductivity measurements. The bars were sintered at 1400 °C for 5h to burn out the pore forming additives. Gold wires were attached to the samples for testing.

Exposure to hydrogen at high temperatures to reduce NiO to Ni(metal) is the last step in fabrication of a porous cermet anode with the final microstructure. Samples used for electrical conductivity tests and BET surface area measurements were first reduced in 100% H_2 at 750 °C for 2–4 h to achieve the cermet anode structure similar to that produced under typical fuel cell conditions.

2.2. *Characterization*

The microstructure of the cermet Ni-BZCYYb anode supported cell was examined using a thermally assisted field emission scanning electron microscope (SEM, LEO 1530). BET surface area per weight (m^2/g) was measured using a Micromeritics Tristar II 3020 surface area analyzer (nitrogen).

The Archimedes method, using water as fluid, was used to measure porosity. Samples were dried overnight and weighed to determine the dry weight. To increase water infiltration for the submerged and wet sample measurements, samples were held under vacuum for 2h before water was added. Surface area per total anode volume (mm^2/mm^3) was calculated using the density calculations taken from data collected by the Archimedes method.

The electrical conductivity was calculated from resistance measurements on Ni-BZCYYb bar samples collected using the 4-probe method.

For fuel cell performance evaluation, the button cell was sealed (Ceramabond 552, Aremco) onto an alumina fuel cell testing fixture, with humidified hydrogen (3% H_2O) as fuel and ambient air as oxidant at 750 °C, 700 °C, and 650 °C. The cell was tested using an Arbin multi-channel electrochemical testing system (MSTAT). A fuel flow rate of 30 sccm was used for testing all cells. Fuel utilization for the best performing cell was approximately 7%, limited primarily by the small

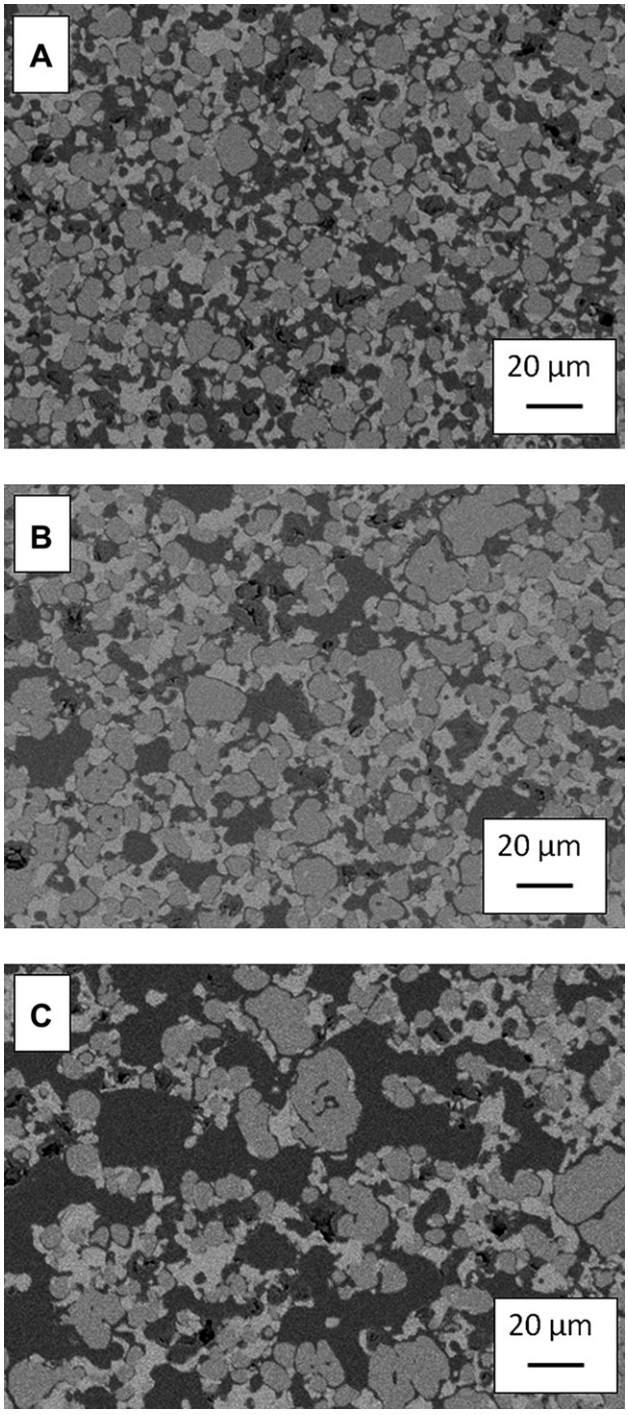

Fig. 1 – SEM (backscattered electron) images (Light-gray = BZCYYb, Mid-gray = Ni (metal), Dark-gray/Black = Epoxy) of A.) Ni-BZCYYb-0, B.) Ni-BZCYYb-10, and C.)Ni-BZCYYb-20 anode microstructures.

Table 1 – Ni-BZCYYb cermet anode porosity and surface area per total anode volume (mm^2/mm^3) based on pore forming content.

Cermet precursor pore former (wt%)	Ni-BZCYYb anode porosity	Surface area (mm^2/mm^3)
0	0.37	2430
10	0.42	2000
20	0.50	1428

effective area of the anode. The cells were first stabilized at 750 °C for about 100h before electrochemical performance test and each condition was repeated in two test cells.

3. Results and discussion

3.1. Ni-BZCYYb anode microstructure

Backscattered electron SEM images of each of the anode samples are shown in Fig. 1. The samples were filled with epoxy and polished to determine the porosity on one focal plane. In the images, the dark-gray phase is epoxy, the light-gray phase is BZCYYb, and the mid-gray phase is Ni(metal). Dark, irregular patches in the images are caused by epoxy pull-out during polishing. Narrow channels between the Ni(metal) and BZCYYb phases can be seen.

Porosity in the Ni-BZCYYb anodes (Fig. 1) increased, as expected, with the amount of pore former added to the precursor powders (Table 1). However, the surface area per total anode volume decreased with porosity. After reduction, the Ni-BZCYYb-20 anode achieved 50% porosity, a value comparable to optimized YSZ cell anodes, which allows us to compare our Ni-BZCYYb-20 anode cell to the optimized YSZ cell from the literature [20]. The Ni-BZCYYb-0 anode achieved 37% porosity, much less than the standard anode porosity in YSZ based cells. The Ni-BZCYYb-0 anode also has the highest surface area per total anode volume. Each anode has a constant Ni:BZCYYb volume ratio, therefore the difference in grain size in the Ni-BZCYYb anodes is due to difference of fabrication with and without pore former.

Porosity is formed in the anode in two ways: first by the burning of pore forming additives during firing, leaving large, round pores, and second by the reduction of NiO to Ni upon exposure to a fuel at high temperatures, leaving long channels of pores between the Ni(metal) phase and the BZCYYb phase. Pore forming additives can create large pores, beneficial to water vapor diffusion through the anode of an oxygen anion conducting SOFC, however, the large round "pockets" of pores have low surface area to volume ratio. Porosity due to pore former burnout is created during the sintering step of the fabrication process. Next, during the reduction of NiO to Ni(metal), a 41.2% reduction in volume of the NiO phase occurs [19]. As oxygen diffuses out of the NiO during the reduction, the nickel particles shrink and "pull-away" from the surrounding BZCYYb framework. Narrow

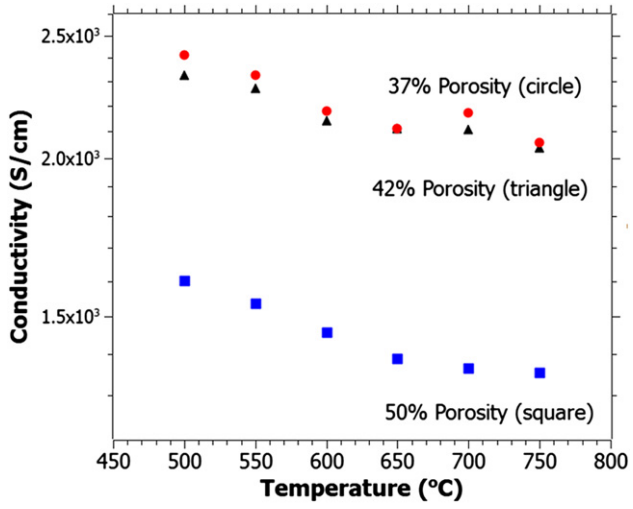

Fig. 2 – Electrical conductivity of Ni-BZCYYb-0 (37% porosity), Ni-BZCYYb-10 (42% Porosity), and Ni-BZCYYb-20 (50% Porosity) under reducing atmosphere measured using a 4-probe technique.

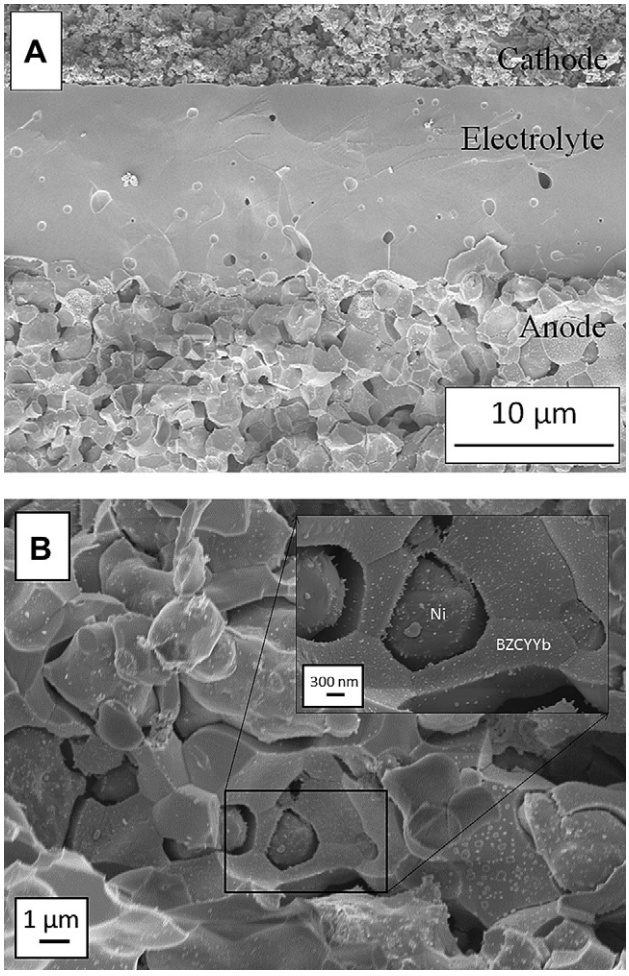

Fig. 3 – A.) SEM (secondary electron) images of a typical cross-sectional view of an anode supported test cell with a configuration of Ni-BZCYYb/BZCYYb/LSCF-BZCYYb (electrolyte thickness = ~15 µm for all test cells) and, B.) Ni-BZCYYb-0 anode microstructure after reduction in hydrogen at 750 °C for 2 h.

channels form between the phases, creating long, narrow pores with high surface area to volume ratio. If pore forming additives are used, both mechanisms create pores in the sample. In the Ni-BZCYYb-0 sample (without pore former), only NiO reduction to Ni(metal) contributed to the anode porosity.

Because pore formation in the NiO reduction occurs after the pore forming additive burn-out (corn starch), the pores formed in the NiO reduction are affected by the pores formed from the pore forming additive (corn starch) burnout. The large, round "pockets" of pores formed by the corn starch allow the oxygen to easily diffuse out of the NiO particles and the anode. However, in the sample with no pores before reduction, the oxygen must take a tortuous path to diffuse out of the NiO particle and the anode. This results in more intricate microstructures on the surface of the nickel particles [19] and more channels of pores surrounding the Ni(metal) particles, which leads to higher surface area.

High surface area per total anode volume is important in anodes for SOFCs. More surface area provides more open sites for anode reactions and can lead to increased length of triple phase boundaries, although quantification of TPB length is difficult and was not attempted in this study. As seen from Table 1, the Ni-BZCYYb-0 anode (37% porosity) developed the largest surface area per volume.

3.2. *Ni-BZCYYb cermet anode electrical conductivity*

Ni-BZCYYb anode electrical conductivity was measured using the 4 probe method (Fig. 2). For optimal anode performance, the nickel phase must provide a contiguous pathway throughout the anode to remove electrons from the hydrogen oxidation process at the TPBs. As porosity increases, the nickel particles are less interconnected, decreasing the electrical conductivity. The conductivity in the anodes of 37% and 42% porosity are sufficient for high anode performance and are also significantly higher than that of the anode with 50% porosity.

The percolation threshold of nickel (metal) in Ni-YSZ cermet anodes is approximately 35 vol% [27]. The electrical conductivity data in this work suggests that the nickel (metal) content in the Ni-BZCYYb cermet anodes with 37% and 42% porosity is above the percolation threshold due to high volume fraction of nickel (metal). However, the significant drop in conductivity of the Ni-BZCYYb-20 sample implies that the nickel (metal) content is in the region of the percolation threshold.

3.3. *SOFC performance*

Fig. 3A reveals a cross-sectional view of a test cell with a configuration of Ni-BZCYYb-0/BZCYYb/LSCF-BZCYYb. All

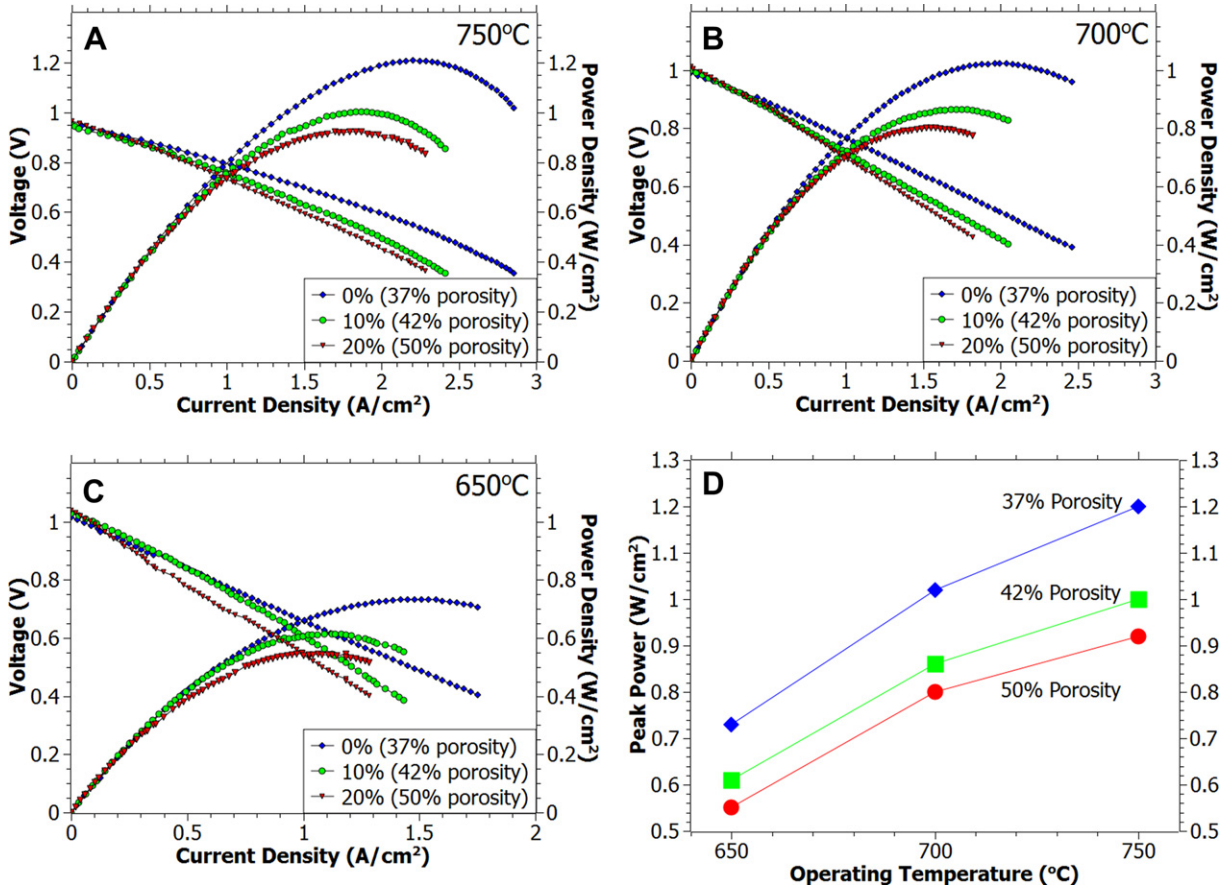

Fig. 4 – Typical I-V curves and calculated power densities for Ni-BZCYYb-0/BZCYYb/LSCF-BZCYYb, Ni-BZCYYb-10/BZCYYb/LSCF-BZCYYb, and Ni-BZCYYb-20/BZCYYb/LSCF-BZCYYb cells at A.) 750 °C, B.) 700 °C, and C.) 650 °C; and D.) A summary of the peak power densities of each cell at all testing temperatures.

the Ni-BZCYYb anode supported cells have a dense electrolyte of ~15 μm thick. The Ni-BZCYYb-0 anode microstructure, after reduction, is represented in Fig. 3B. The high magnification inset reveals the narrow channel porosity formed after NiO reduction to Ni (metal). Fig. 4 shows some typical performance data at 650 °C, 700 °C, and 750 °C for three cells based on BZCYYb with anodes of different porosity and microstructure: (A) a Ni-BZCYYb-0 anode (without pore former), (B) a Ni-BZCYYb-10 anode (with 10% pore former), and (C) a Ni-BZCYYb-20 anode (with 20% pore former). The detailed microscopic features of the anodes with different amount of pore former are shown in Fig. 1. The highest performance is observed in the cell with the Ni-BZCYYb-0 anode (without pore former, 37% porosity). Peak power densities of 1.20 W/cm^2, 1.02 W/cm^2, and .73 W/cm^2 were observed at 750 °C, 700 °C, and 650 °C, respectively. At 750 °C, the cell with the Ni-BZCYYb-0 anode outperformed the cell with the Ni-BZCYYb-10 anode by 20% and the one with the Ni-BZCYYb-20 anode cell, with the anode porosity comparable to conventional YSZ based cell anodes, by 30%. The peak power densities observed under different conditions are summarized in Fig. 4D.

The straightness of the I-V curves suggest that concentration polarization in these cells is relatively small, an indication of sufficient porosity for gas transport of fuel and reaction products in all three samples. The electrical conductivity data suggests that increased contiguity of the nickel phase in the 37% porosity sample does not lead to a significant improvement in electrical conductivity over the 42% porosity sample. Therefore, the small improvement in electrical conductivity may have little impact on anode performance. Accordingly, the increased performance in the cell with the anode fabricated without the use of pore former is attributed primarily to the unique microstructure which forms during NiO reduction when no pore former is present. It appears that the narrow channel pores derived from reduction of NiO to Ni (metal) alone would be sufficient for hydrogen transport through the anode for proton conducting SOFCs. The cell with Ni-BZCYYb-0 anode was tested at 0.7 V for over 100 h at 750 °C and showed no obvious degradation. The stability test data is plotted in Fig. 5.

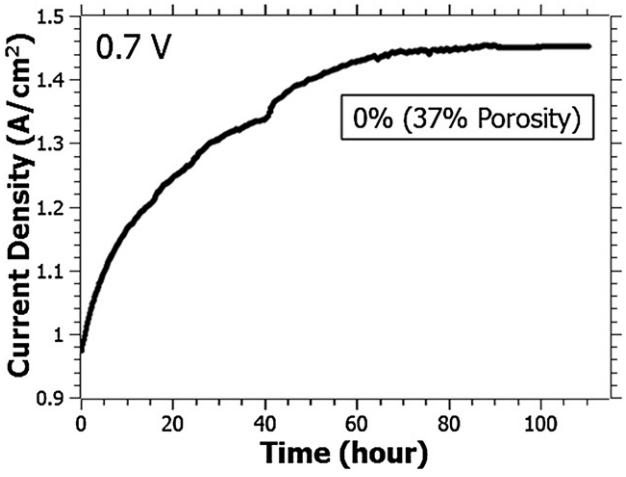

Fig. 5 – BZCYYb based fuel cell with Ni-BZCYYb-0 anode (without pore former) tested at 0.7 V and 750 °C for 100h.

4. Conclusions

Because water is formed at the cathode side for a proton conducting SOFC, the anode for such a cell requires less porosity than oxygen anion conducting SOFCs, where the water is formed at the anode side. The reduction of NiO to Ni(metal) alone produces sufficient porosity for fast fuel diffusion to the triple phase boundary reaction sites in the anode for SOFCs with significant proton conduction. The microstructure formed by Ni(metal) "pull-away" from the ion-conducting phase during reduction forms narrow channels of pores instead of large, round pores left by pore forming additives. The increased surface area (and TPBs) per volume in the anode fabricated with no pore former, Ni-BZCYYb-0 (37% porosity), leads to increased activity for SOFC reactions. The high surface area, low porosity Ni-BZCYYb-0 anode was tested alongside anodes fabricated using pore forming additives and a large increase in performance was observed at temperature ranges of 650 °C–750 °C. Peak power densities of 0.73 W/cm^2 and 1.2 W/cm^2 were observed at 650 °C and 750 °C, respectively, for proton conducting SOFCs based on low porosity, high specific surface area nickel-cermet anodes. Therefore, the conventional porosity (~55%) for YSZ based oxygen anion SOFC anodes should not be used in proton conducting SOFCs. This study finds that a significantly lower porosity (~37%) is optimal for SOFCs based on proton conductors.

Acknowledgments

This material is based upon work supported by the HetroFoaM Center, an Energy Frontier Research Center funded by the U.S. Department of Energy, Office of Science, Office of Basic Energy Sciences under Award Number DE-SC0001061 as well as work supported by the National Science Foundation under Grant No. DGE-1148903.

REFERENCES

[1] Williams MC, Strakey JP, Surdoval WA. The US department of energy, office of fossil energy stationary fuel cell program. J Power Sources 2005;143:191–6.
[2] Liu MF, Choi YM, Yang L, Blinn K, Qin WT, Liu P, et al. Direct octane fuel cells: a promising power for transportation. Nano Energy 2012;1:448–55.
[3] Steele BCH, Heinzel A. Materials for fuel-cell technologies. Nature 2001;414:345–52.
[4] Singhal SC. Solid oxide fuel cells for stationary, mobile, and military applications. Solid State Ionics 2002;152:405–10.
[5] Liu M, Lynch ME, Blinn K, Alamgir FM, Choi Y. Rational SOFC material design: new advances and tools. Mater Today 2011; 14:534–46.
[6] Yang L, Choi Y, Qin WT, Chen HY, Blinn K, Liu MF, et al. Promotion of water-mediated carbon removal by nanostructured barium oxide/nickel interfaces in solid oxide fuel cells. Nat Commun 2011;2:357.
[7] Zuo C, Zha S, Hatano M, Uchiyama M, Liu ML. $Ba(Zr_{0.1}Ce_{0.7}Y_{0.2})O_3$ as electrolyte for low-temperature SOFCs. Ads Mater 2006;18:3318–20.

[8] Yang L, Wang SZ, Blinn K, Liu MF, Liu Z, Cheng Z, et al. Enhanced sulfur and coking tolerance of a mixed ion conductor for SOFCs: BaZr0.1Ce0.7Y0.2-xYbxO3-delta. Science 2009;326:126–9.
[9] Kreuer KD. Aspects of the formation and mobility of protonic charge carriers and the stability of perovskite-type oxides. Solid State Ionics 1999;125:285–302.
[10] Manning PS, Sirman JD, DeSouza RA, Kilner JA. The kinetics of oxygen transport in 9.5 mol % single crystal yttria stabilised zirconia. Solid State Ionics 1997;100:1–10.
[11] Fabbri E, Pergolesi D, Traversa E. Electrode materials: a challenge for the exploitation of protonic solid oxide fuel cells. Sci Technol Adv Mat 2010;11.
[12] Iwahara H, Yajima T, Ushida H. Effect of ionic-radii of dopants on mixed ionic-conduction (H++O2-) in Baceo3-based electrolytes. Solid State Ionics 1994;70:267–71.
[13] Iwahara H, Yajima T, Hibino T, Ushida H. Performance of solid oxide fuel-cell using proton and oxide-ion mixed conductors based on Bace1-Xsmxo3-Alpha. J Electrochem Soc 1993;140:1687–91.
[14] Bonanos N, Knight KS, Ellis B. Perovskite solid electrolytes - Structure, transport-properties and fuel-cell applications. Solid State Ionics 1995;79:161–70.
[15] Zhou XL, Liu LM, Zhen JM, Zhu SC, Li BW, Sun KN, et al. Ionic conductivity, sintering and thermal expansion behaviors of mixed ion conductor BaZr0.1Ce0.7Y0.1Yb0.1O3-delta prepared by ethylene diamine tetraacetic acid assisted glycine nitrate process. J Power Sources 2011;196:5000–6.
[16] Iwahara H, Uchida H, Tanaka S. High-Temperature type proton conductor based on Srceo3 and its application to solid electrolyte fuel-cells. Solid State Ionics 1983;9-10:1021–5.
[17] Coors WG, Manerbino A. Characterization of composite cermet with 68 wt.% NiO and BaCe(0.2)Zr(0.6)Y(0.2)O(3-delta). J Membr Sci 2011;376:50–5.
[18] Atkinson A, Barnett S, Gorte RJ, Irvine JTS, McEvoy AJ, Mogensen M, et al. Advanced anodes for high-temperature fuel cells. Nat Mater 2004;3:17.
[19] Suzuki T, Hasan Z, Funahashi Y, Yamaguchi T, Fujishiro Y, Awano M. Impact of anode microstructure on solid oxide fuel cells. Science 2009;325:852–5.
[20] Zhao F, Virkar AV. Dependence of polarization in anode-supported solid oxide fuel cells on various cell parameters. J Power Sources 2005;141:79–95.
[21] Fergus JW. Solid oxide fuel cells: materials properties and performance. Boca Raton: CRC Press; 2009.
[22] Singhal SC, Kendall K. High temperature solid oxide fuel cells: fundamentals, design and applications. Amsterdam: Elsevier; 2003.
[23] Bonanos N. Transport-properties and conduction mechanism in high-temperature protonic conductors. Solid State Ionics 1992;53:967–74.
[24] Bi L, Fabbri E, Traversa E. Effect of anode functional layer on the performance of proton-conducting solid oxide fuel cells (SOFCs). Electrochem Commun 2012;16:37–40.
[25] Zunic M, Chevallier L, Radojkovic A, Brankovic G, Brankovic Z, Di Bartolomeo E. Influence of the ratio between Ni and BaCe(0 9)Y(0 1)O(3-delta) on microstructural and electrical properties of proton conducting Ni-BaCe(0) (9)Y(0) (1)O(3-delta) anodes. J Alloys Compd 2011;509:1157–62.
[26] Liu MF, Gao JF, Dong DH, Liu XQ, Meng GY. Comparative study on the performance of tubular and button cells with YSZ membrane fabricated by a refined particle suspension coating technique. Int J Hydrogen Energy 2010;35: 10489–94.
[27] Lee JH, Moon H, Lee HW, Kim J, Kim JD, Yoon KH. Quantitative analysis of microstructure and its related electrical property of SOFC anode, Ni-YSZ cermet. Solid State Ionics 2002;148:15–26.